Faraday Discussions

Accepted Manuscript

This manuscript will be presented and discussed at a forthcoming Faraday Discussion meeting. All delegates can contribute to the discussion which will be included in the final volume.

Register now to attend! Full details of all upcoming meetings: http://rsc.li/fd-upcoming-meetings

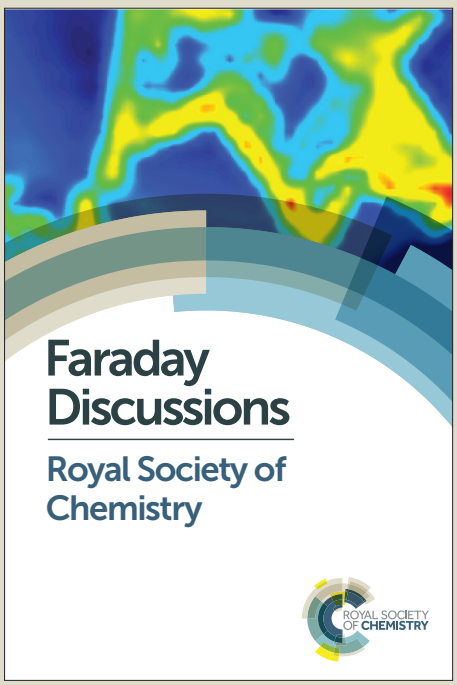

This is an *Accepted Manuscript*, which has been through the Royal Society of Chemistry peer review process and has been accepted for publication.

Accepted Manuscripts are published online shortly after acceptance, before technical editing, formatting and proof reading. Using this free service, authors can make their results available to the community, in citable form, before we publish the edited article. We will replace this *Accepted Manuscript* with the edited and formatted *Advance Article* as soon as it is available.

You can find more information about *Accepted Manuscripts* in the Information for Authors.

Please note that technical editing may introduce minor changes to the text and/or graphics, which may alter content. The journal's standard Terms & Conditions and the Ethical guidelines still apply. In no event shall the Royal Society of Chemistry be held responsible for any errors or omissions in this *Accepted Manuscript* or any consequences arising from the use of any information it contains.

ROYAL SOCIETY OF CHEMISTRY

www.rsc.org/faraday_d

Faraday Discussions

ARTICLE

A transition metal oxofluoride offering advantages in electrocatalysis and potential use in applications

Received 16th November 2015,
Accepted 2nd December 2015

DOI: 10.1039/x0xx00000x

www.rsc.org/

H. Svengren[a*], N. Torapava[b], I. Athanassiadis[a], S. I. Ali[a] and M. Johnsson[a]

The recently described solid solution $(Co,Ni,Mn)_3Sb_4O_6F_6$ has proved stable and efficient as catalyst for electrocatalytic water oxidation. The end component $Co_3Sb_4O_6F_6$ was found to be most efficient maintaining a current density of j = 10 mA cm^{-2} at an overpotential of 443mV with good capability. At this current density O_2 and H_2 were produced in the ratio 1 : 2.1 without loss of Faradaic current against a Pt-cathode. A morphological change of the crystallite surface was observed already after 0.5 h, however, still after 64.5 h the overall shape and size of the small crystallites were unaffected and the electrolyte contained only 0.02 at% Co. It was also possible to conclude from *in situ* EXAFS measurements that the coordination around Co was not changed. The oxofluorides express both hydrophilic and hydrophobic surface sites, incorporates a flexible metalloid element and offer the possibility of a mechanism that differ from other inorganic catalytic pathways previously described.

Introduction

The environmental consequence of human consumption of non-renewable energy is rapidly increasing the demand for advancement in efficient utilization of sustainable energy and storage. Efficient storage is today mostly focusing on batteries and reduced fuels such as hydrogen or hydrocarbons. Rechargeable batteries have undergone tremendous development during recent years and are continuously searching new routes for increasing battery life time, charge-discharge efficiency and improved energy density.[1] Research has accordingly led to new and intriguing discoveries in electrode materials including a new class of fluorine-based materials as high capacity electrodes. Fluorine-based materials have historically been discarded as electrode materials due to their insulating properties; therefore this class of compounds have to a great extent been overlooked in search for efficient electrodes. Sufficient conductivity can be achieved for practical applications by addition of a conductive agent such as carbon into the electrode paste that has opened up for finding new electrode materials. The perovskite–type 3d–transition metal trifluorides, MeF_3, have exhibited high capacity ion exchange cathode materials.[2] Transition metal oxofluorides typically in the family of MeOF have proven as high capacity active cathodes for Li–ion batteries.[3] Research in the area of hydrogen fuel generation through water splitting has gained focus on the oxygen evolution reaction (OER) which constitutes a bottleneck in the overall reaction.[4] Efforts have been made to find ways to lower the activation energy by a catalytically functional electrode. Noble metals, transition metals, and their salts are well known water oxidation catalysts (WOC's) and are also implemented in traditional industrial hydrogen processing.[5] It has been shown how Co^{II} and Ni^{II} from aqueous solution form catalysts during *in situ* electrolysis with phosphate and borate ions.[6] Oxides[7] containing first row transition metals such as Fe, Mn, Co, and Ni or polyoxymetalates[8] and hydroxides[9] have been identified as active catalysts. Recent work proposes that in metal oxides it is a metal hydroxide in the form of an oxyhydroxide that constitute the active site.[7a,10] Change in morphology after exfoliation of oxyhydroxides generating layered double hydroxide (LDH) nanosheets with a hierarchical structure increased the active surface area enhancing gas release and consequently improved the catalytic performance.[11] An outstanding example of a catalytic system optimized for water oxidation is the core cluster $[CaMn_4O_5]$ in the oxygen evolving complex of nature's photosystem II (PSII). The cluster exhibits five oxo-bridges linking the metals to form a distorted cubane structure with an additional Mn site.[12] Reactant H_2O is channelled through a protein environment to the inorganic core complex to preferred oxygen sites in the mechanistic cycle. One oxygen atom is more weakly bonded and may adopt a lower negative charge than a valence of –II and hence be important in the mechanism of dioxygen formation.[12] Inspired by this crystal structure, oxides with oxygen coordination in a cubic arrangement around the Mn or Co atoms, with or without incorporated redox-inactive metals such as Ca, La, and Li, have been studied extensively.[13] These systems show high

[a] *Department of Materials and Environmental Chemistry, Stockholm University, SE-106 91 Stockholm, Sweden.*
[b] *Max IV Laboratory, Lund University, SE-221 00 Lund, Sweden.*
* Corresponding author, tel: +46-8-162386, fax: +46-8-152187, email: henrik.svengren@mmk.su.se.
Electronic Supplementary Information (ESI) available: Table of weight in amounts used in the experiments, SEM micrographs, images on the analytical set up, ECSA plot and XAFS data graphs PXRD patterns. See DOI: 10.1039/x0xx00000x

activity, involving alternation of the metal valence electrons to a higher state in oxo-bridging to $–OH_2$, –OH, –O, and –O–O species during the catalytic cycle.[6a,7a,13a,14] A special class of compounds is transition metal-metalloid-oxofluorides, MeMiOF. Our group has synthesized and characterized several such compounds and among them is the solid solution $(Co_xNi_{1-x})_3Sb_4O_6F_6$ [15] and $(Co_{0.86}Mn_{0.14})_3Sb_4O_6F_6$, the latter presented as a novel compound in this work. The compound exhibits a cubic arrangement of the active transition metal that oxo-bridge to the metalloid Sb with possible catalytic participation. Recently we demonstrated that relatively hard (270HV0.1, Mohs 3.5-4) and fairly large crystals (0.3-0.5mm) can easily be synthesized, see Figure 1.[16] We can in this study present electrochemical characterization of $(Co_xNi_{1-x})_3Sb_4O_6F_6$, (x = 1, 0.75, 0.5, 0.25, 0) and the novel compound $(Co_yMn_{1-y})_3Sb_4O_6F_6$ (y = 0.86). The studies include linear sweep voltammetry (LSV) polarization curves, chronopotentiometry at a current density of 10 mA cm^{-2}, Tafel slope, kinetics, relative comparison of electrochemical surface area (ECSA), Faradaic efficiency of O_2 and H_2 production, long term durability with metal leaching analysis, SEM-EDS and X-ray absorption fine structure (XAFS) analyses. As the MeMiOF materials exhibit both hydrophilic and hydrophobic sites on the interface, we further discuss the catalytic mechanism.

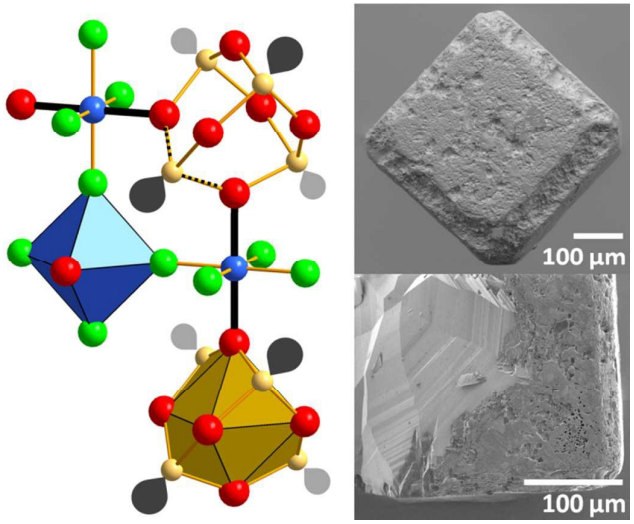

Figure 1 The crystal structure (left) of $Co_3Sb_4O_6F_6$ is made up by slightly distorted $[CoO_2F_4]$ octahedra that are corner sharing via F atoms. The O atoms connect further to $[Sb_4O_6]$ cages, highlighting that there are only two possible locations for oxo-bridging for each cobalt atom. The O–Co–O–Sb–O–Co–O oxo-bridge is illustrated with black/dashed bonds. Co (blue), O (red), Sb (yellow) with its lone pair (gray) and F (green). A single crystal (right), the fractured surface reveals the dense bulk.

Results and discussion

Electrochemical evaluations of heterogeneous catalysts in functionalized working electrodes have many independent factors to account for as described by McCrory *et al.*[24] In this study efforts were dedicated to formulate a systematic and repeatable method for fabricating working electrodes. The aim of this effort is to minimize variation in electrocatalytic performance originating from electrode inhomogeneity in respect to particle distribution, catalyst density and working electrode area. Thin film application of a paste in optimal consistency proved to be the best method for the oxofluoride compounds. The electrodes were in this way formulated to yield repeatable electrodes for electrochemical evaluation within this study and not optimized for benchmarking *vs.* electrodes manufactured in other ways such as layered double hydroxides grown directly on the current support.[11a] We therefore think that it is not appropriate to directly compare figure of merits, such as overpotentials with electrodes assembled in other ways. As a general summary the study from McCrory *et al.* found that many promising WOC's had overpotentials between 330-500 mV at a current density j = 10 mA cm^{-2}.[24b] The electrochemical analysis of the different compounds were repeated with three different electrodes and presented as the average. Electrolytes were chosen based on two criteria; (i) a neutral pH stable buffer and (ii) an electrolyte used commercially. Phosphate buffer at pH 7 has shown positive effects in catalysis using cobalt.[6,16] A negative effect could arise from the fact that the conjugate PO_4^{3-} base exhibit strong coordination and low solubility to transition metals, for example $Co_3(PO_4)_2$ K_{sp} = 10^{-35},[25] $Ni_3(PO_4)_2$ K_{sp} = 10^{-32} and $Mn_3(PO_4)_2$ K_{sp} = 10^{-24},[26] which may spoil the native crystals or decrease the electrocatalytic performance. Potassium hydroxide is already a commercially used electrolyte for electrolysis of water[5] and can be expected as a realistic candidate in future solar fuel device.[24] The alkali electrolyte was chosen to pH 14 in 1 M KOH.

Linear scan voltammogram and Tafel slope

Electrochemical activity evaluated with linear scan voltammetry compensated for internal resistance (R_i) of the different compounds is shown in Figure 2. The compound yielding the highest current response to the overpotential scan is the pure cobalt compound $Co_3Sb_4O_6F_6$ and the catalytic activity then decreases with decreasing Co-content (x-value) for the solid solution series. The ranking order of the compounds from high to low was found to be: x=1 > y=0.86 > x=0.75 > CoO/Co_3O_4 > x=0.5 > x=0.25 > x= 0. The control electrode not containing catalyst showed insignificant response. The two most active compounds were chosen for comparing Tafel plots in the potential range where low current response starts to increase. From the Tafel slope the overpotential required for a current density j > 0 is minimum 340 mV for $Co_3Sb_4O_6F_6$ and 359 mV for $(Co_{0.86}Mn_{0.14})_3Sb_4O_6F_6$, respectively. Interestingly, the very first potential scan on a pristine electrode shows a current response around 1.5 – 1.6

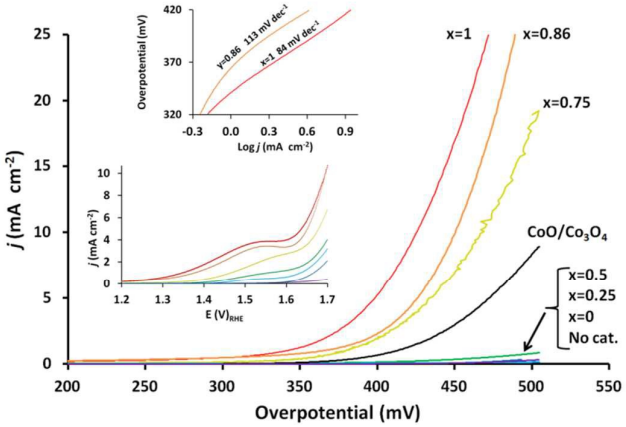

Figure 2 R_i-compensated polarization curves from preconditioned electrodes that have reached a stable state at a linear scan rate of 2 mVs^{-1}. The upper insert shows Tafel plots for the two most active phases $Co_3Sb_4O_6F_6$ at 84 mV dec^{-1} and $(Co_{0.86}Mn_{0.14})_3Sb_4O_6F_6$ at 113 mV dec^{-1}. The lower insert shows redox waves deduced for $Co^{II} \rightarrow Co^{III} \rightarrow Co^{IV}$ seen only at the very first scan on a pristine electrode. Electrolyte was 1 M KOH.

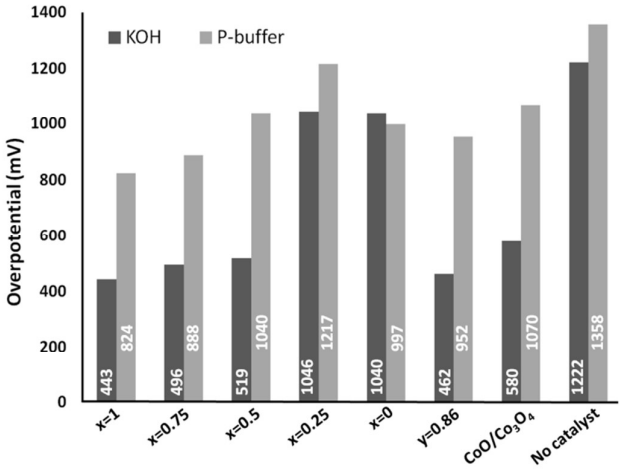

Figure 3 Overpotentials η required at the current density j = 10 mA cm^{-2}.

V_{RHE} in proportion to the cobalt content and for the following scans this characteristic disappears. The Co-oxide electrode did not show this characteristic. An explanation for this could be that the pristine crystal surface exposing Co^{II} is oxidized to higher state Co^{III} and possibly Co^{IV} for the first oxidation scan creating a redox-wave and henceforth an active surface in equilibrium with its surrounding. Co-oxide did not show this characteristic behavior, the compound was established to $Co^{II}O/Co^{III}{}_3O_4$ in a ratio which is already a redox-stable phase. This behavior shows how important it is to precondition the electrodes to a stable state prior to characterization.

Chronopotentiometry and overpotential

The current density (j) output for a 10% efficient solar water splitting device is generally expected to j = 10 mA cm^{-2}.[24] We have in this study chosen the required overpotential (η) at this current density for assessment of electrocatalytic activity in water oxidation. The overpotential was determined in chronopotentiometric mode with an initial applied current density of j = 1 mA cm^{-2} for 5 min followed by an increase to j = 10 mA cm^{-2} for 10 minutes and presented as an average from three experiments. The overpotential for respective compound is presented in Figure 3 in two different electrolytes with different pH; 0.1 mol/dm^3 phosphate buffer pH 7 and 1.0 mol/dm^3 potassium hydroxide pH 14. The large difference in η between the two electrolytes can be addressed to both a large difference in conductivity (11.5 mS for 0.1 M phosphate buffer and 240 mS for 1 M KOH) as well as different mechanistic difference in the presence of PO_4^{3-} ions and pH conditions. The lowest overpotential η = 443 mV required for j = 10 mA cm^{-2} is addressed to the compound with x = 1. Interestingly, the phase with x=0 requires lower η than x=0.5 and x=0.75 in phosphate buffer. This is the only deviation from the general trend that higher fraction of cobalt gives proportionally higher activity. Graphical visualization of data from chronopotentiometry in 1 M KOH is seen in Figure 4 and the insert show a single experiment for the most electrocatalytic compound x=1 that was continued for 5 hours demonstrating the long term stability with an increase of only ~10mV. All compounds show the same type of kinetics in KOH comparable to the one in Figure 4, however, in phosphate buffer the curves have different kinetic appearance, seen in Figure 5. The required potential for j = 1 mA cm^{-2} does not incite other redox-events than the expected slow oxidation of water. When the current density applies to j = 10 mA cm^{-2} the required potential raises and redox-events are seen.

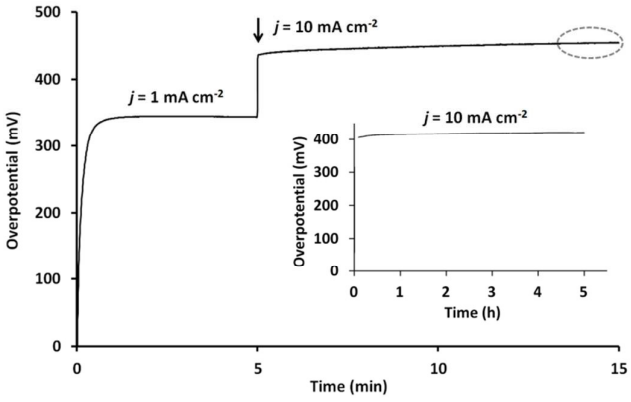

Figure 4 Chronopotentiometry to evaluate the overpotential η at j = 10 mA cm^{-2} for x=1 in 1 M KOH. The dotted ellipse highlights the data range used for calculation of average overpotential from three of the electrodes presented in Figure 3. The insert shows the stability during 5 hours.

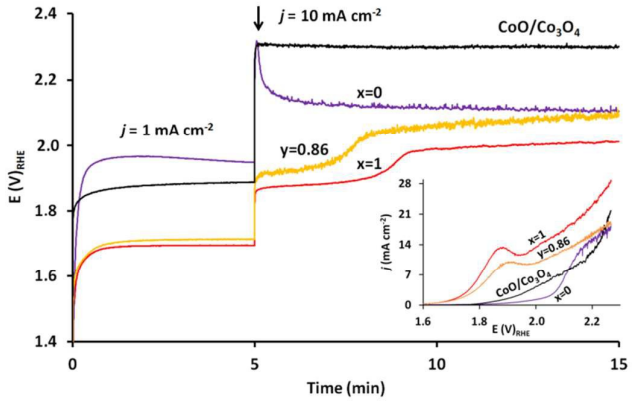

Figure 5 Chronopotentiometry of the two most active compounds x=1 and y=0.86 in relation to x=0 and CoO/Co_3O_4 in 0.1 M phosphate buffer at pH 7 showing 1) the trend in redox wave characteristic for $Co^{II} \rightarrow Co^{III} \rightarrow Co^{IV}$ – Co-Pi in phosphate buffer, 2) activation of Ni and 3) insignificant change of CoO/Co_3O_4 powder that have reached a stable state. The insert shows the same trends from R_i-compensated LSV (scan rate 2 mVs^{-1}) using preconditioned electrodes that have reached a stable state.

The two most active compounds x=1 and y=0.86 shows a current flow requiring lower initial potential that ceases after approximately 3 min and the potential is increased to a higher level. Correspondingly, a redox peak can be seen in the inserted voltammogram. This is most likely addressed to a flow of charge originating from $Co^{II} \rightarrow Co^{III} \rightarrow Co^{IV}$. Different from the redox event assumed to take place in the very first LSV in KOH seen in Figure 2, the behavior seen in Figure 5 takes place on a preconditioned electrode that has reached stable state prior to analysis and the redox event takes place repeatedly. It is therefore attempting to conclude that the PO_4^{3-} ion is involved in the reaction. Such an event could be that when the potential allows Co^{III} species, less coordination to PO_4^{3-} occurs, but when the potential decreases $Co^{III} \rightarrow Co^{II}$ formation is pushed to the right to form $Co^{II}{}_3PO_4$ due to a low value of K_{sp}. Nickel shows a different behavior, it appears to require a higher potential to activate catalysis, and the initiated current flow requires a lower potential thereafter. This event is reflected in the inserted voltammogram where a higher potential needs to induce the current flow that then increases relatively fast. A conclusion on the difference of two electrolytes is that phosphate buffer appears to have more interactions on a mechanistic level on the oxofluorides than KOH and that this possibly would obstruct the catalytic performance.

Electrocemically Active Surface Area

The Electrochemical Active Surface Area (ECSA) was estimated by analyzing the capacitive current associated with the double layer charging from scan rate dependence of R_i-compensated cyclic voltammograms (CV) in the non-Faradaic region. The true value of ECSA in cm^2 is obtained from the ratio of double layer capacitance C_{dl} (mF) to the specific capacitance C_s (mF cm^{-2}) of the sample. C_s is unknown for the present samples and beyond the scope of this work to determine. We therefore approximate the ECSA to the double layer capacitance per electrode geometric surface area C_{dl} (mF cm^{-2}) to offer a relative comparison of the surface activity of the two most active compounds x=1 and y=0.86 in relation to x=0 and CoO/Co_3O_4 presented in Figure 6. The difference in C_{dl} is relatively large between the two most active compounds that are close in the Co-content, possibly could the 14% Mn on the metal site have altered the capacitance of the compounds. This relatively large difference is not seen in activity results from LSV in Figure 2 or CP in Figure 3 where the electrochemical character is more similar. It was expected that the CoO/Co_3O_4 electrode should show a relatively large value of C_{dl} due to the large difference in particle size 0.1-50 µm for the crushed oxofluorides and 0.1-1 µm for the Co-oxide powder. It can be concluded from LSV, CP, CV (ECSA) investigations that the compounds $Co_3Sb_4O_6F_6$ and $(Co_{0.86}Mn_{0.14})_3Sb_4O_6F_6$ exhibit higher electrocatalytic activity than the electrode made from CoO/Co_3O_4 that served as benchmark for the electrodes. However, taking into account the complexity of fabricating electrodes to a very similar molar ratio of Co per surface area makes it difficult to determine exactly how much higher the activity is for the two most active oxofluoride compounds compared to the oxide electrode.

Leaching

A true catalyst should per definition not be consumed during the catalytic reaction and only act to lower the activation

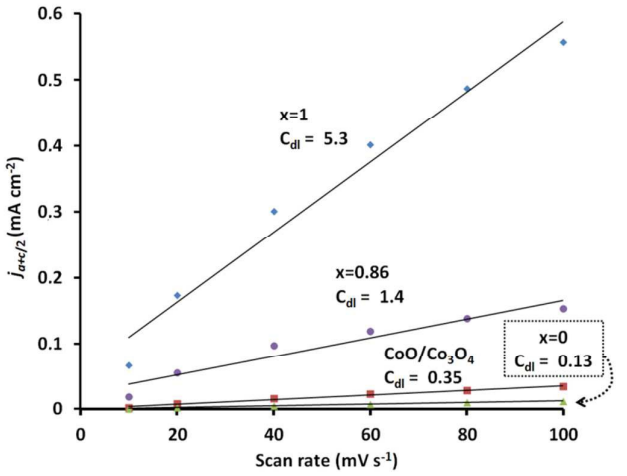

Figure 6 Electrochemical Active Surface Area (ECSA) approximated to the double layer capacitance C_{dl} (mF cm^{-2}) for relative comparison of surface activity of the two most active compounds x=1 and y=0.86 in relation to x=0 and CoO/Co_3O_4 in 1 M KOH. Data was obtained from R_i-compensated voltammograms.

energy of the reaction catalyzed. One way to evaluate this is long term experiments studying the phase stability and leaching. The most active catalyst, x = 1, was chosen for studies at an applied current density j = 10 mA cm^{-2} during 64.5 h in 1 M KOH electrolyte. The electrolyte was thereafter analyzed with ICP-MS resulting in the low leakage of 0.02 at%. The same x = 1 phase, this time with 10 mg native crystals, was placed in 1 M KOH electrolyte without an applied potential for 20 h and removed for single crystal XRD to investigate the phase stability in the strong alkaline environment. This experiment did not show any phase transformation. We conclude from the two experiments that the crystals under *in-situ* conditions show good stability with low leakage and the 1 M KOH electrolyte does not provoke any phase change. Furthermore, we measured the Co-content in an electrode used in the experiments. 1 cm^2 area of an x = 1 electrode was first heated for 30 min in concentrated HNO_3 at 120°C to dissolve the metal and the solution was subsequently analyzed with ICP-MS. The total cobalt content was determined to be 14.9 µmol that is 85.5% of the calculated amount.

Kinetics

The Kinetics of the catalysis in the studied oxidation reaction $2H_2O \rightarrow O_2 + 4H^+ + 4e^-$ on the anode containing $Co_3Sb_4O_6F_6$ required an overpotential η = 443 mV at steady current density of j = 10 mA cm^{-2} obtained by CP presented in Figure 4. This reaction also involves the process of electron and mass transport diffusion at the interface between the crystal surface and the electrolyte. Conditioned that the cell circuits at Faradaic current, the same is valid for the reaction $2H^+ + 2e^- \rightarrow H_2$ at the Pt cathode. The temperature dependent kinetics for the experimental conditions adopted in this study at an applied oxidation overpotential η_{OX} = 443 mV was estimated. A water bath surrounding the cell was used to let the temperature be varied three times with fast, medium and slow temperature change between 16 – 44 °C in the electrolyte. In respect to the reaction $2H_2O \rightarrow O_2 + 4H^+ + 4e^-$ the recorded current density j / nF (n = 4 e^-), was plotted against the temperature as 1/T (K) using the Arrhenius equation $k = b \cdot e^{-Ea/RT}$ and the result is presented in Figure 7. According to the calculated rate constant k (Faraday/4 [mol O_2 equivalents] cm^{-2} s^{-1}), approximately 20 degrees increase in temperature will double the O_2 yield in the presented temperature range. Mass activity in respect of [O_2 eq.] related to k was calculated at three different temperatures 16°C, 25°C and 44°C to 6.5, 8.8 and 15.8 nmol [O_2 eq.] per mg x = 1, respectively, in the present electrode formulation. The insert in Figure 7 shows the data sets from the three different temperature changes in an Arrhenius plot.

Faradaic efficiency

The claim of having a compound catalyzing the reaction $2H_2O \rightarrow O_2 + 4H^+ + 4e^-$ should accordingly be proved by gas evolution and the Faradaic efficiency determined. This can be done by measuring oxygen evolution. However, electrolysis of water according to $2H_2O \rightarrow O_2 + 2H_2$ by using an electrocatalytic counter electrode large enough not to bottleneck the overall electron flow, consequently rising the overpotential, should also be established by the simultaneous detection of H_2 gas. To evaluate this a gas tight electrochemical single chamber cell was connected to a mass spectrometer and employed with a WE of $Co_3Sb_4O_6F_6$ having a geometric surface area of 14.9 cm^2, a reference electrode, double Pt mesh as a CE and 1 M KOH electrolyte. The set up and results are presented in Figure 8.

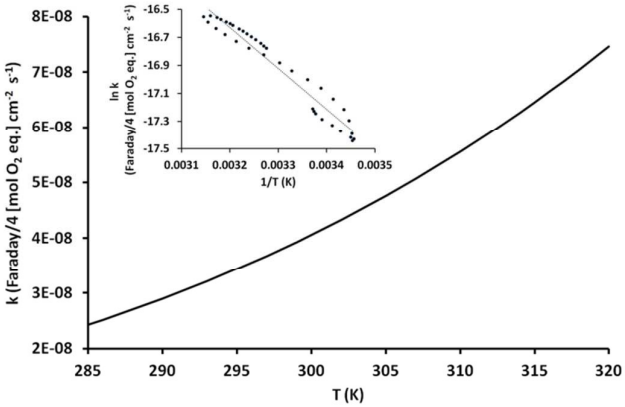

Figure 7 Kinetic behavior of $Co_3Sb_4O_6F_6$ in 1 M KOH showing the temperature dependence of the rate constant k at an applied overpotential of η = 443 mV. The insert shows the Arrhenius plot combined from three data sets and the corresponding regression line from which k was calculated.

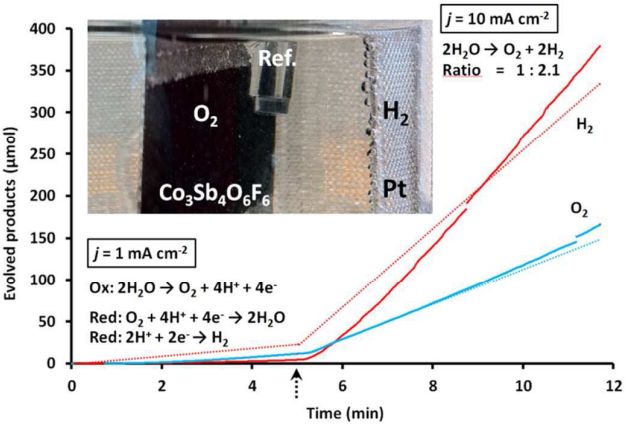

Figure 8 Faradaic efficiency of $Co_3Sb_4O_6F_6$ plotted as evolved products (smooth line) at an applied current density of j = 1 mA cm^{-2} for the first 5 min followed by an increase to j = 10 mA cm^{-2} (indicated by an arrow) in relation to the expected production (dotted line). The ratio $O_2 : H_2$ was determined to 1 : 2.1. The Faradaic efficiency was measured to 107% for O_2 and 114% for H_2; an experimental tolerance on absolute amounts of gaseous and aqueous products in the cell should be applied.

Faradaic efficiency at an applied current density of j = 1 mA cm^{-2} for the first 5 min revealed that oxygen evolved as expected but hydrogen did not evolve sufficiently. This leads to the conclusion that the cell potential at j = 1 mA cm^{-2} was too small for reduction of $2H^+ + 2e^- \rightarrow H_2$ highlighting the importance of performing Faraday efficiency studies at a high enough current to make the oxidation potential valid for Faradaic splitting of water. Another redox reaction must balance the current flow; the reaction that is most likely in a single cell chamber is the reverse recombination reaction $O_2 + 4H^+ + 4e^- \rightarrow 2H_2O$. After 5 min, current density was increased to j = 10 mA cm^{-2} and the required oxidation potential measured to 1.728 V_{RHE}. At this current density the cell potential was enough to evolve both O_2 and H_2 gas in a 1 : 2.1 proportion at an oxidation overpotential η = 498 mV. The slightly higher overpotential in this experiment compared to the CP results at η = 443 mV presented in Figure 3 could originate in errors when scaling the WE 15 times in geometric size and the fact that the reference electrode was not in an optimal position due to the practical reasons in the gas tight cell. The Faradaic efficiency was measured to 107% for O_2 and 114% for H_2 that is above the expected Faradaic production, however, the experiment involve a tolerance on the absolute amounts of gaseous and aqueous products in the cell. The fact that the Faradaic efficiency was larger than the expected but still at an acceptable ratio of 1 : 2.1 made it possible to conclude that the evolutions of H_2 and O_2 were satisfactory.

Mechanism

Several mechanistic studies of organic- and inorganic catalysts propose that two active metal atoms connected via an oxo-bridge co-operate when bonding to water. Reaction intermediates like –OH_2, –OH, –O, and –O–O and finally molecular oxygen form during the catalytic cycle that involves changes in valence states of the active metals; in case of Co it means a change between +III and +IV.[7a,14a] In the present oxofluoride compounds the metal (Co, Ni, Mn) is octahedrally coordinated to four F and two O, see Figure 1. The oxygen atoms bridge further to Sb and are potential sites for the catalytic reactions. If those oxygens play a role during the catalytic reaction it means that they are involved in the formation of new bonds to reactant intermediates that would break the oxo-bridges in between Co and Sb, such a process would thus destroy the crystal structure. However, this does not match with the fact that the crystals performs well as catalysts both chemically[16] and electrochemically for a long time period. The electrocatalytic activity show a quite stable oxidation potential over 5 h at an applied current density of j = 10 mA cm^{-2}, seen in Figure 4. The cell potential decreased slightly during a period of 64.5 h showing a low leakage of 0.02 at% Co in the alkaline electrolyte. The electrodes were analysed with SEM-EDS and in high magnification the surface morphology of the crystallites changed from being smooth in the electrode before electrolysis to become rough already after 0.5 h. This rough surface morphology seems then not to change with time and is similar for the electrode used for 64.5 h, see Figure 9. EDS results show that all ingoing elements are present in comparable ratios both in an outer thin edge and in the centre of a crystal, see Figure 10 and Table 1. This result supports that the composition of the crystal and its outer layer, that seems to be amorphous, have the same composition. Also the XAFS experiments obtained at a current density of j = 1 mA cm^{-2}, see Figure 11 did show that the crystalline phase persist after applied potential, supporting the findings of the stable crystallite shape seen in SEM.

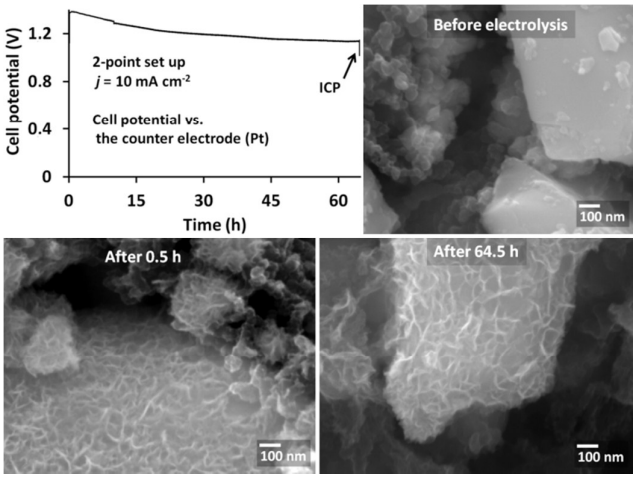

Figure 9 The cell potential during 64.5 h after which the electrode was withdrawn from the electrolyte for ICP analysis and SEM studies. The image before electrolysis shows a homogenous smooth crystallite surface, after 0.5 h of electrolysis a morphological change of the surface is seen and after 64.5 h of electrolysis the morphology appears the same.

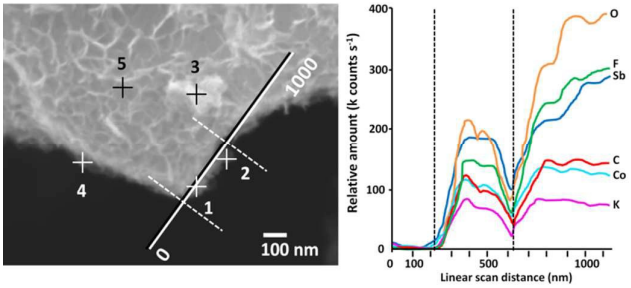

Figure 10 SEM-EDS analysis of a $Co_3Sb_4O_6F_6$ crystallite on the electrode surface after 64.5 h of use with an applied current density of j = 10 mA cm^{-2}. The change in surface morphology is seen in the picture. The EDS linear scan spectra shows that all the elements are represented in the thin surface. The result was also observed (Table 1) with point spectra analysis at the markers 1-5.

Table 1. SEM-EDS elemental composition (at%) of the sample points 1-5 shown in Figure 11.

Point	C	O	F	K	Co	Sb	Ratio
1	34	27	17	2	13	7	1 : 1.7
2	27	16	16	3	22	17	1 : 1.3
3	27	29	28	1	9	6	1 : 1.6
4	39	15	14	2	17	12	1 : 1.4
5	17	28	37	1	8	8	1 : 1.0
Std.	8.5	7.2	9.9	0.9	5.7	4.5	

The XAFS spectra reflected most likely the vast bulk crystal in the 200 µm thick, 1 cm^2 large electrode, rather than the thin electrochemically active interface, as we could not detect any difference in the oxidation state of neither cobalt nor nickel when the potential was on or off. A mechanism where both Co and Sb are involved appears as an alternative when considering the electrocatalytic performance and the results from XAFS, SEM, and EDS. When Co^{II} oxidise to Co^{III} or Co^{IV} it form a stronger bond to oxygen in the bridge over to Sb^{III}. This Sb – O bond may then weaken allowing the coordination around Sb^{III} to change. Sb^{III} is flexible and can adopt both trigonal pyramidal coordination (three bonds) like in the present oxofluoride compounds and see-saw coordination (four bonds). If a forth weak bond is formed from Sb to $–OH_2$ it will lead to that the –Co–O–Sb–O– oxo-bridge is further weakened resulting in longer Sb-O bond distances. The weaker Sb-O bonds may be important for the dioxygen formation

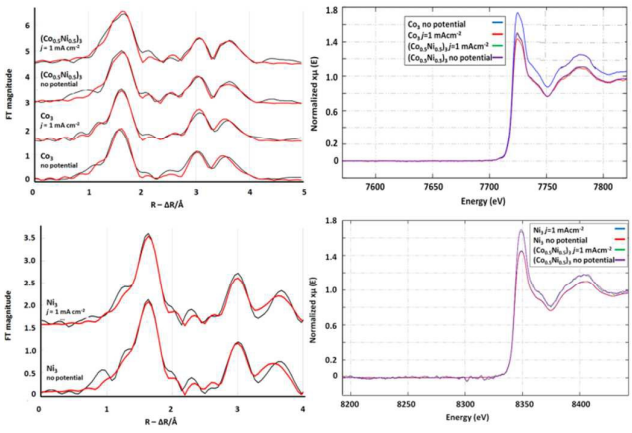

Figure 11 In situ measured EXAFS (left) and XANES (right) of Co and Ni K edge, respectively, from x=1, x=0.5 and x=0 with and without an applied current of 1 mA cm^{-2} in 0.1 mol dm^{-3} phosphate buffer pH 7. The XAFS plot shows Fourier transforms with the calculated model (red line) and the experimental data (black line). FT data are offset by +2.

process and hydroxide and intermediate oxygen species can thus be stabilized. Formation of molecular oxygen from water is a process that is not thermodynamically favored and a gaseous phase would be less energy demanding if a non-polar surface is accessible in the highly polar electrolyte. Hence F could also passively mediate the reaction by lowering the formation energy of the dioxygen molecule. Fluorine may also play a role in directing water molecules to the oxo-bridges. In this study there is thus evidence for that the oxofluoride phase persists in shape, activity and composition with a morphological change in the surface and there are no indications that the compound collapse to form *e.g.* Co-oxide nanoparticles. Being open for the possibility that other catalytically active species *e.g.* hydroxides may form the mechanism outlined here will require least change from the native structure and the role of F would not be negative but instead positive.

Experimental

The hydrothermal synthesis of compounds within the solid solution $(Co_xNi_{1-x})_3Sb_4O_6F_6$ (x = 1, 0.75, 0.5, 0.25, 0) were made according to Hu *et al.*[15] Also the isostructural compound $(Co_yMn_{1-y})_3Sb_4O_6F_6$ (y = 0.86) was synthesized under similar conditions starting with the off-stoichiometric mixture of 4 mmol CoF_2 (STREM Chemicals), 1 mmol MnF_2 (Sigma-Aldrich) and 1 mmol Sb_2O_3 (Sigma-Aldrich) together with 2 ml of deionized water. Crystals where manually separated from the synthesis product for further investigations. Single crystal X-ray diffraction experiments (XRD) were carried out by using a Bruker D8 Venture diffractometer equipped with a PHOTON 100 CMOS detector. Data integration, including the application of a correction for oblique incidence, was done with software package SAINT.[17] Absorption correction was applied by the computer program SADABS.[18] Structure solution is done by Superflip.[19] Structure refinements were made by use of JANA2006.[20] Powder X-ray data (PXRD) were collected on a Panalytical X'Pert PRO powder X-Ray diffractometer in Bragg-Brentano geometry with Cu-Kα radiation. Scanning electron microscopy (SEM) studies were made by use of a JEOL JSB-7000F equipped with an energy-dispersive spectrometer (EDS). The working electrodes were prepared by mixing powder of each corresponding crystal phase in the molar proportion 889 µmol (approx. 250 mg, 75 wt%) of transition metal content with 333.13 mg (approx. 10 wt%) carbon black (Imerys, Super C65), 50 mg (approx. 15 wt%) polyvinylidenfluorid (Arkema, Kynar FLEX 2801) and 0.8 ml of N-methyl-2-pyrrolidone (VWR/Prolabo). The suspension was ground in a mortar to a homogenous paste, applied with doctor blade technique using a film applicator of 16.5 mm width and 200 µm film thickness on a carbon fibre paper (Freudenberg, GDL-H23) and dried at 60 °C for three hours. The thin film was typically 10 cm long and were cut to electrodes having a catalytic film area of 1 cm^2. An electrode for benchmarking was prepared from commercially available cobalt oxide (ABCR GmbH). The phase composition was found to be CoO/Co_3O_4 = 0.54 / 0.46 from PXRD data. The same molar proportion of transition metal (Co

+ Ni + Mn) per electrode unit area was used for all the oxofluoride electrodes, comparable to the CoO/Co_3O_4 electrode. Because of the smaller wheight in volume of CoO/Co_3O_4 powder, the total paste volume suitable for the thin film applicator was maintained by adding carbon black and PVDF in the same ratio as for the oxofluoride electrodes. The particles size of the CoO/Co_3O_4 appeared in average smaller and more uniform, approximately 0.1 - 1µm, than the oxofluoride ranging from approximately 0.1 - 50 µm. Serving as a reference an electrode was also prepared from carbon black and PVDF without presence of catalyst. Two electrolytes were prepared; potassium hydroxide solution 1.00 mol/dm^3 pH 13.99 from KOH (VWR Chemicals) and phosphate buffer 0.1 mol/dm^3 pH 6.91 from Na_2HPO_4 (Sigma-Aldrich) and KH_2PO_4 (J.T. Baker Chemical Co.). Electrochemical characterization was performed using a potentiostat (BioLogic, model SP-50) with standard three point set up; working electrode (WE), counter electrode (CE) of Pt-mesh and an Ag/AgCl reference electrode (ALS Co.) except in the experiment lasting for 64.5 h and the *in situ* XAFS experiment where a two point set up was used composed of a working electrode and a counter electrode (Pt-mesh) with the cell voltage referring to the counter electrode. The electrodes were placed in the centre of a single chamber open cell containing 35 ml of electrolyte and stirred with a magnet at 2500 rpm placed under the WE. Prior to investigation the electrodes were preconditioned to reach a stable state using cyclic voltammetry (CV) until negligible change in current response, 15 cycles between 0 – 1.6 $V_{Ag/AgCl}$ in phosphate buffer and 6 cycles between 0 – 0.7 $V_{Ag/AgCl}$ at a scan rate of 20 mVs^{-1}. Ohmic drop was measured using the current interrupt (CI) method and the internal resistance (R_i) was subsecquently corrected for by employing the BioLogic software for the following potentiostatic techiques; R_i-compensated linear sweep voltammetry (LSV) at a scan rate of 2 mVs^{-1} used for Tafel plot and R_i-compensated CV estimating the electrochemical active surface area (ECSA). ECSA was analyzed using CV in the non-Faradaic window between 0.05 – 0.15 $V_{Ag/AgCl}$ (1 M KOH) by measuring the capacitive current originating from the double layer charging depending on the different scan rates 10, 20, 40, 60, 80, 100 mVs^{-1}. Potential scans were held at each potential vertex for 10 s before the subsequent scan. The double layer capacitance (C_{dl}) was calculated by plotting Δj (j_a-j_c) against the scan rate where the slope of the fitted linear regression corresponds to $2C_{dl}$. Chronopotentiometry (CP) was perfomed at a current density (j) of 1 mA cm^{-2} an 10 mA cm^{-2}. The potential scale has been calculated versus the reversible hydrogen electrode (RHE) using the Nernst equation $E_{RHE} = E_{Ag/AgCl} + 0.059$ pH + 0.209, where the reference electrode filled with NaCl electrolyte at 3 mol/dm^3 and has a potential offset of +0.209 V_{SHE}. Overpotential was calculated as η (V) = E_{RHE} – 1.23 V. In the Faradaic efficiency experiment a mass spectrometer (Pfeiffer, model Thermostar GSD320-QMG220) was used to quantify the evolved amounts, n (moles), of molecular H_2 and O_2 during an applied current density of 1 mA cm^{-2} for 300 s followed by an increase to 10 mA cm^{-2} for 402 s interrupted due to rising pressure. Calculations were made according to Faradaic efficiency = n_{gas} / Q(nF)$^{-1}$, where Q (C) is the charge passed, n is the number of electrons, n_{gas} is the amount gas (mol O_2 or H_2) in the reaction. The reactions were performed in a 440 cm^3 gas tight single chamber containing 185 ml KOH electrolyte at room temperature with a working electrode exposing 14.9 cm^2 of catalytic film and stirred with a magnet at 1000 rpm. The EXAFS data of nickel (Ni) and cobalt (Co) K edge were recorded at the wiggler beamline I811 at the Max IV Laboratory, Lund University, Lund, Sweden. The facility operated at 1.5 GeV and a maximum current of 250 mA. The EXAFS station was equipped with a Si [111] double crystal monochromator. Working electrodes of $(Co_xNi_{1-x})_3Sb_4O_6F_6$, (x = 1, 0.5, 0) were cut to an area of 1 cm^2 and placed in a 1 mm thick plastic frame covered with Kapton film constituting an electrochemical cell with a volume 0.23 cm^3. Phosphate buffer of 1.0 mol dm^{-3} at pH 7 was used as electrolyte. The cell was connected in a two point set up. The experiments were performed in the transmission and fluorescence mode using gas filled ion chambers. Higher order harmonics were reduced by detuning the second monochromator crystal to 40% for both Ni and Co of maximum intensity at the end of the scan. The energy scale of the X-ray absorption spectra was calibrated by assigning the first inflection point of the K edges of Ni to 8331.49 eV and of Co to 7708.78 eV.[21] The EXAFSPAK program package was used for data treatment.[22] For each sample 1-2 scans were averaged after energy calibration by means of the EXAFSPAK program package. The experimental spectra were Fourier-transformed using the k-window over the k-space ranging between 2 and 14 Å^{-1}. The theoretical phase shift and backscattering amplitudes were obtained using the known crystal structures of $Co_3Sb_4O_6F_6$ and $Ni_3Sb_4O_6F_6$. The calculated EXAFS structure parameters were refined using FEFF ver. 7.02 based on models considering only single scattering contributions.[23] The distances, R, and the Debye-Waller factors, σ^2, were refined simultaneously. The amplitude reduction factors, S_0^2, and the shift in threshold energy, ΔE, were varied as a global parameter in the fit procedure. Determination of Co-levels in the KOH electrolyte while using an electrode based on oxofluorides with x = 1 was made by ICP-MS analysis (Thermo X-Series 2). The sample from the electrolyte was acidified with 1% HNO_3 and the electrode sample having a catalytic area of 1 cm^2 was heated to 120°C for 30 min diluted and quantified against internal standards.

Conclusions

The recently described oxofluoride solid solution $(Co_xNi_{1-x})_3Sb_4O_6F_6$ and the novel compound $(Co_yMn_{1-y})_3Sb_4O_6F_6$ (y = 0.86) were characterized with electrochemical methods for water oxidation catalysis. Efforts were put on forming a repeatable method for electrode formulation. Two electrolytes were studied, 1 M KOH (pH 14) and 0.1 M phosphate buffer (pH 7). An electrode with similar formulation and with comparable molar ratio of Co to the oxofluorides was prepared as a benchmark from cobalt oxide powder having a composition of 54 mol% CoO and 46 mol% Co_3O_4. Linear scan voltammetry reveals a ranking order so that the activity

decreases with decreasing amount of Co for both electrolytes. Higher current response to potential was seen in the alkaline electrolyte and Tafel plots comparable for the two most active compounds was calculated at 84 mV dec^{-1} for x = 1 and 113 mV dec^{-1} for y = 0.86. The characteristic redox wave $Co^{II} \rightarrow Co^{III} \rightarrow Co^{IV}$ was seen only at the very first scan in the alkaline electrolyte but for the phosphate buffer the redox wave remained. This observation is likely to depend on the low solubility product of $Co^{II}_3(PO_4)_2$ (K_{sp} 10^{-35}) forcing most Co^{III} and Co^{IV} to go back to the low oxidation state when the potential decreases. Overpotentials were determined for all compounds by chronopotentiometry at the current density j = 10 mA cm^{-2}. In general the overpotential was lower for the alkaline electrolyte than the phosphate electrolyte, however, one should take into account the difference in conductivity between the 1 M KOH at 240 mS and phosphate buffer at 11.55 mS. In alkaline electrolyte, the two most active compounds operated at overpotentials of 443 mV for x = 1 and 462 mV for y = 0.86 in comparison to 580 mV for CoO/Co_3O_4. The overpotential for x = 1 was maintained over 5 h with a small increase of ~10 mV. In a longer experiment lasting for 64.5 h using a two point set up measuring the cell potential referring to the counter Pt-electrode the cell potential did not increase. After 64.5 h the electrolyte was analysed with ICP showing a leakage of only 0.02 at%. As an indication, the study by McCrory *et al.* concluded that several promising WOC's did show an overpotential in the range 330-500 mV, and that the complexity in different electrode compositions has to be considered.[24b] Hence no direct comparison with other types of electrodes was made in this study for the benefit of the internal ranking. Electrochemical active surface area was approximated to C_{dl} and did show a similar trend as the activity with x = 1 being highest at 5.3 mF cm^{-2}, y = 0.86 1.4 mF cm^{-2} and CoO/Co_3O_4 0.35 mF cm^{-2}, respectively. At an applied overpotential of 443 mV for x = 1 using chronoamperometry, there was a temperature dependence of the output current roughly equivalent to doubling the O_2 yield for a 20 °C temperature increase. Faradaic efficiency using mass spectrometry at an applied current density of j = 10 mA cm^{-2} was determined to a ratio $O_2 : H_2$ of 1 : 2.1 with no Faradaic current loss. Investigations by SEM shows that even small crystallites survive in shape and size after 64.5 h of electrolysis at j = 10 mA cm^{-2} but that the surface has a change in morphology. SEM-EDS and EXAFS shows that the surface interface still contains all the elements of the parent phase and that the metal coordination does not change after the potential was applied. Speculating in that there could be diversity in mechanistic pathways for different catalysts to obtain an oxygen evolution reaction, Sb could play an active role in the present oxofluorides if changing from trigonal pyramidal to see-saw coordination with weaker bonds to oxygen, consequently having larger bond distances. This could be important for O_2 formation in a –O–Co–O–Sb–O– cluster coordinating reactant H_2O and intermediate species during reaction. However, such a transformation would require flexibility in the crystalline phase and possibly the observed morphological surface change could be an amorphous active interface. As a final remark the present oxofluoride show good stability and is a well performing WOC. Further studies of the mechanism will be carried out.

Acknowledgements

Pär Hjelmquist for performing ICP-MS analysis. Kjell Jansson for assistance with the SEM imaging. The Swedish Research Council for financial support.

References

1 J. Goodenough, *Energy Environ. Sci.*, 2013, **7**, 14.
2 (a) M. Nishijima, I. Gocheva, S. Okada, T. Doi, J. Yamaki and T. Nishida, *J. Power Sources*, **150**, A1318. (b) F. Badway, F. Cosandey, N. Pereira, and G. Amatucci, *J. Electrochem. Soc.*, 2003, **110**, 6474-6502.
3 (a) I. Gocheva, I. Tanaka, T. Doi, S. Okada and J. Yamaki, *Electrochem. Comm.*, 2009, **11**, 1583. (b) N. Pereira, F. Badway, M. Wartelsky, S. Gunn, and G. Amatucci, *Electrochem. Soc.*, 2009, **156**, A407. (c) M. Reddy, S. Madhavi, G. Subba Rao and B. Chowdari, *J. Powder Sources*, 2006, **162**, 1312.
4 (a) N. Lewis and G. Nocera, *PNAS*, 2006, 103, 15729. (b) T. Cook, D. Dogutan, S. Reece, Y. Surendranath, T. Teets and D. Nocera, *Chem. Rev.* 2010**, 110***,* 6474. (c) M. Walter, E. Warren, J. McKone, S. Boettcher, Q. Mi, E. Santori and N. Lewis, *Chem. Rev*., 2010, **110**, 6446.
5 B. Tilak, P. Lu, J. Colman, S. Srinivasan in *Comprehensive Treatise of Electrochemistry, Vol. 2* (Eds.: J. Bockris, B. Conway, E. Yeager, R. White), Plenum, New York, 1981, pp. 1-97.
6 (a) Y. Surendranath, M. Kanan and D. Nocera, *J. Am. Chem. Soc.*, 2010, **132**, 16501-16509. (b) M. Kanan, D. Nocera, *Science*, 2008, **321**, 1072. (c) Y. Surendranath, M. Dinca, D. Nocera, *J. Am. Chem. Soc.*, 2009, **131**, 2615. (d) M. Kanan, Y. Surendranath, D. Nocera, *Chem. Soc. Rev.*, 2009, **38**, 109. (e) A. Esswein, Y. Surendranath, S. Reece and D. Nocera, *Energy Env. Sci.*, 2011, **4**, 499-504. (f) M. Dinca, Y. Surendranath, D. Nocera, *PNAS,* 2010, **107**, 10337. (g) M. Kanan, J. Yano, Y. Surendranath, M. Dinca, V. Ychandra and D. Nocera, *J. Am. Chem. Soc.*, 2010, **132**, 13692-13701.
7 (a) J. Gerken, J. McAlpin, J. Chen, M. Rigsby, W. Casey, R. Britt and S. Stahl, *J. Am. Chem. Soc.*, 2011, **131**, 14431. (b) L. Bloor, P. Molina, M. Symes and L. Cronin, *J. Am. Chem. Soc*, 2014, **136**, 3304. (c) Y. Gorlin and T. Jamillo, *J. Am. Chem. Soc.*, 2010, **132**, 13612. (d) Q. Yin, J. Tan, C. Besson, Y. Geletii, D. Musaev, A. Kutznetsov, Z. Luo, K. Hardcastle and C. Hill, *Science*, 2010, **328**, 342. (e) M. Wiechen, I. Zaharieva, H. Dau and K. Kurz, *Chem. Sci.*, 2013, **3**, 2330. (f) I. Zaharieva, P. Chernev, M. Risch, K. Klingan, M. Kohlhoff, A. Fischer and H. Dau, *Energy Environ. Sci.*, 2012, **5**, 7081. (g) M. Lyons and M. Brandon, *Int. J. Electrochem. Sci.*, 2008, **132**, 1386. (h) M. Lyons and M. Brandon, *Int. J. Electrochem. Sci.*, 2008, **132**, 1425. (i) A. Singh, S. L. Chang, R. K. Hocking, U. Bach and L. Spiccia, *Energy Environ. Sci.*, 2013, **6**, 579. (j) J. Rosen, G. Hutchings and F. Jiao, *J. Am. Chem. Soc.,* 2013, **135**, 4516. (k) J. Kirner, J. Stracke, B. Gregg, R. Finke, *ACS Appl. Mater. Interfaces*, 2014, **6**, 13367. (i) J. McAlpin, T. Stich, H. William and R. Britt, *Coord. Chem. Rev.*, 2012, **256**, 2445. (m) A. Han, H. Wu, Z. Sun, H. Jia, P. Du, *Phys. Chem. Chem. Phys.*, 2013, **15**, 12534-12538. (n) N. Chou, P. Ross, A. Bell and T. Tilley, *Chem. Sus. Chem.*, 2011, **4**, 1566. (o) C-C. Yang, T. Eggenhuisen, M. Wolters, A. Agiral, H. Frei, P. Jongh, K. Jong and G. Mul, *Chem. Cat. Chem.*, 2013, **5**, 550. (p) M. Bajdich,

M. Garcia-Mota, A. Vojvodic, J. Nørskov, A. Bell, *J. Am. Chem. Soc.*, 2013, **135**, 13521.
8 (a) J. Soriano-Lopez, S. Goberna-Ferron, L. Vigara, J. Carbo, J. Poblet and J. Galan-Mascaros, *Inorg. Chem.* 2013, **52**, 4753. (b) J. Stracke and R. Finke, *ACS Catal.*, 2013, **3**, 1209. (c) J. Stracke and R. Finke, *ACS Catal.,* 2014, **4**, 909. (d) J. Stracke and R. Finke, *J. Am. Chem. Soc.,* 2011, 133, 14872.
9 (a) G. Elizarova, G. Zhidomirov and V. Parmon, *Catalysis Today,* 2000, **58**, 71-88. (b) X. Wang, H. Luo, H. Yang, P. Sebastian and S. Gamboa, *Int. J. Hydrogen Energy*, 2004, **29**, 967-972.
10 (a) L. Trotochaud, J. Ranney, K. Williams and S. Boettcher, *J. Am. Chem. Soc*, 2012, **134**, 17253. (b) M. Gong, Y. Li, H. Wang, Y Liang, J. Wu, J. Zhou, J. Wang, T. Regier, F. Wei and H. Dai, *J. Am. Chem. Soc*, **13**, 135, 8452. (c) R. Doyle, I. Godwin, M. Brandon and M. Lyons, *Phys. Chem. Chem. Phys*., 2013, **15**, 13737. (d) I. Godwin and M. Lyons, *Electrochem. Commun.,* 2013, **32**, 39. (e) K. Bediako, B. Lassalle-Kaiser, Y. Surendranath, J. Yano, V. Yachandra and D. Nocera, *J. Am. Chem. Soc*, 2012, **134**, 6801. (f) Y. Surendranath, D. Lutterman, Y. Liu and D. Nocera, *J. Am. Chem. Soc.*, 2012, **134**, 6326.
11 (a) H. Liang, F. Meng, M. Cabán-Acevedo, L. Li, A. Forticaux, L. Xiu, Z. Wang and S. Jin, *Nano Lett*. 2015, **15**, 1421. (b) F. Song and X. Hu, *Nat. Comm.* 2014, **5**, 4477.
12 Y. Umena, K. Kawakami, J-R. Shen and N. Kamiya, *Nature*, 2011, **473**, 55.
13 (a) U. Maitra, B. Naidu, A. Govindaraj and C. Rao, *Proc. Nat. Acad. Sci.,* 2013, **110**, 11704. (b) N. McCool, D. Robinson, J. Sheats, G. Dismukes, *J. Am. Chem. Soc*, 2011, **133**, 11446. (c) M. Symes, D. Lutterman, T. Teets, B. Anderson, J. Breen and D. Nocera, *Chem. Sus. Chem.*, 2013, **6**, 65. (d) E. Tsui, R. Tran, J. Yano and T. Agapie, *Nat. Chem.*, 2013, **5**, 293.
14 (a) M. Zhang, M. Respinis and H. Frei, *Nature Chem.*, 2014, **6**, 362. (b) J. McAlpin, Y. Surendranath, M. Dinca, T. Stich, S. Stoian, W. Casey and D. Nocera, *J. Am. Chem. Soc.*, 2010, **132**, 6882. (c) A. Indra, P. Menezes, I. Zaharieva, E. Baktash, J. Pfrommer, M. Schwartze, H. Dau and M. Driess, *Angew. Chem. Int. Ed.*, 2013, **52**, 13206.
15 S. Hu, M. Johnsson, P. Lemmens, D. Schmid, D. Menzel, J. Tapp and A. Möller, *Chem. Mater.*, 2014, **26**, 3631.
16 H. Svengren, S. Hu, I. Athanassiadis, T. Laine and M. Johnsson, Chem. Eur. J., 2015, **21**, 12991
17 *Bruker manual,* AXS Inc*.,* Madison, 2012.
18 G. Sheldrick, *SADABS 2008/1*, Univ. of Göttingen, Göttingen, 2008.
19 V. Petricek, M. Dusek, and L. Palatinus. *Kristallogr.,* 2014, **229**, 345.
20 L. Palatinus and G. Chapius, *J. Appl. Crystallogr*., 2007, **40**, 786.
21 A. Thompson, D. Attwood, E. Gullikson, M. Howells, K. Kim, J. Kirz, J. Kortright, I. Lindau, P. Pianatta, A. Robinson, J. Scofield, J. Underwood, D. Vaughan, G. Williams and H. Winick. *X-ray Data Booklet*, Berkeley, California, 2001.
22 G. George and I. Pickering. *EXAFSPAK – A Suite of Computer Programs for Analysis of X-ray Absorption Spectra*, SSRL, Stanford, 1993.
23 (a) A. Filliponi, *J. Phys.: Condens. Matter*, 1994, **6**, 8415. (b) A. Filipponi, A. Di Cicco and C. Natoli, *Phys Rev B*, 1995, **52**, 15122.
24 (a) C. McCrory, S. Jung, J. Peters and T. Jaramillo, *J. Am. Chem. Soc.*, 2013, **135**, 16977. (b) C. McCrory, S. Jung, I. Ferrer, S. Chatman, J. Peters and T. Jaramillo, *J. Am. Chem. Soc*, 2015, **137**, 4347.
25 P. Kelter, M. Mosher, A. Scott, *Chemistry the Practical Science*, Houghton Mifflin Company, Boston, 2009, p. A15
26 D. Nordstrom, L. Plummer, D. Langmuir, E. Busenberg, H. May, B. Jones and D. Parkhurst, *WATEQ4F thermodynamic database*, wwwbrr.cr.usgs.gov/projects/GWC_coupled/phreeqc; W. Ball and D. Nordstrom, *Chemical Modeling of Aqueous Systems II*, A.C.S. Symp. Ser. 416 (eds. D. C. Melchior and R. L. Basett), Am. Chem. Soc., Washington, 1990, pp. 398-413; WATEQ4F, *User's manual with revised thermodynamic data base and test cases for calculating speciation of major, trace and redox elements in natural waters*, U.S. Geological Survey Open-File Report 90-129, pp. 185.